SEECCM III
3rd South-East European Conference on Computational Mechanics-
an ECCOMAS and IACM Special Interest Conference
M. Papadrakakis, M. Kojic, I. Tuncer, V. Papadopoulos (eds.)
Kos Island, Greece, 12–14 June 2013

NUMERICAL ANALYSIS ABOUT THE INFLUENCE OF INAPPROPRIATE SHAPE OF THE CROSS-SECTION OF MICROCHANNELS IN LAMINAR FLOW

Fabiano Da Rosa Hollweg[1], Rejane De Césaro Oliveski[2], Marcelo Dalla Corte[2]

[1] Universidade do Vale do Rio dos Sinos
Av. Unisinos, 950, São Leopoldo, RS 93022-000, Brazil
e-mail: fabiano.hollweg@gmail.com

[2] Universidade do Vale do Rio dos Sinos
Av. Unisinos, 950, São Leopoldo, RS 93022-000, Brazil
decesaroo@gmail.com, marcelodallacorte@gmail.com

Keywords: microchannels, Poiseuille, Nusselt, CFD.

Abstract. *In the past decades, several experimental investigations performed to the hydrodynamics and heat transfer in microscale laminar flow have showed divergences to the Darcy friction factor and the Poiseuille and Nusselt numbers, when the results obtained for the same ones were compared to those provided by classical theory. There are reports of deviations to the Darcy friction factor and the Poiseuille and Nusselt numbers attributed to geometric imperfections at the cross-section of the microchannels. The aim of this numerical study is to analyze how the hydrodynamic and heat transfer characteristics in single-phase laminar flow, of a fluid with constant thermophysical properties, can be affected by imperfections at the cross-section of the microchannels. The results obtained for single-phase laminar flow of water in microchannels with imperfections at the cross-section are compared to those obtained for a geometrically perfect microchannel through Poiseuille and Nusselt numbers. Deviations at Poiseuille and Nusselt numbers due to imperfections at the cross-section of the microchannels were verified. The results showed that Nusselt number is more sensitive to shape of the cross-section of the microchannels than Poiseuille number. This study showed that knowledge about the geometrical shape of the cross-section of the microchannels is important to determine properly the hydrodynamic parameters of the flow, such as Poiseuille number. This study was carried out through computational fluid dynamics (CFD) and the numerical model made up by mass conservation, Navier-Stokes and energy equations.*

1 INTRODUCTION

In recent years, the reduction of electronic devices in several application fields, such as biomedicine, chemistry and electronics has been providing high efficiency related to the space in equipments. At the same time, this reduction in physical space is counterweighted by the high performance required at the refrigeration systems in such equipment. Therefore, thermal control is one of the most critical areas for the development of modern microelectronic devices [1-5].

A lot of experimental studies [1, 2, 5-21], besides theoretical [22-24] and numerical studies [5, 25-28], have been carried out, in the past decades, seeking to investigate the hydrodynamics and heat transfer characteristics in microscale. The results obtained in several of these studies show diversions among themselves and, also, with the conventional theory. In general, the reported divergences can be viewed through analysis of the Darcy friction factor or the Poiseuille and Nusselt numbers, when the results obtained for them are compared to those provided by conventional theory [1, 2, 19, 21].

There are reports of friction factors and Poiseuille numbers either above [2, 6, 12, 23, 26] or below [7-10, 16] of what is predicted by the classical theory, as well as in good agreement with it [2, 11-14, 16, 18]. Some researchers attribute the deviations found for the friction factor or Poiseuille number to variations of the cross-section of microchannels due to the surface roughness [6, 12, 14, 17]. Other researchers attribute these deviations to deformations existing in the cross-section of the microchannels [2, 21], to aspect ratio of channels [2, 5, 8, 17] and, also, to scaling effects, such as viscous dissipation [19, 26] and electrokinetic effect [22, 23], for example. Uncertainty analysis carried out in several experimental studies attribute to the inaccuracy in the measurement of hydraulic diameter of the microchannels as one of the main reasons of errors in determining the friction factor and Poiseuille number in microscale flow [1, 16, 19-21]. Additionally, there are reports [8, 18] of deviations to the friction factor that showed dependence on the Reynolds number.

In relation to microscale heat transfer, some researchers have reported results obtained for the Nusselt number in good agreement with the classical theory [25, 30-33]. However, other researchers have indicated that differences in rates and coefficients of heat transfer, as well as in Nusselt number, can be related to the flow velocity and fluid temperature [16, 34-36], the Reynolds number [9], the heat transfer conjugated [2, 37-39], the viscous dissipation [16, 20, 26, 40, 41], the surface roughness [42], the aspect ratio of microchannels [5, 43] and the conductivity of the material that compose them [2, 37-39], besides experimental uncertainties [4, 30-33, 44]. Some numerical studies [45, 46] showed that the Nusselt number is more sensitive to the shape of the cross-section of the microchannels in comparison to other parameters, such as surface roughness, for example. Furthermore, there are numerical and theoretical studies that consider simplifications which differ a lot from what actually should occur experimentally as, for example, the negligence of viscous dissipation in numerical model [28, 47], the true boundary condition at the limits [44] and the consideration of the fluid with constant thermophysical properties, in general.

Thereby, geometrical parameters of the microchannels, experimental uncertainties and the presence of several possible scaling effects, at once, complicate the identification of probable error sources in experimental studies in this application area. Therefore, the use of numerical techniques can be advantageous in the study of flow in microscale, since significant effects in this field, such as surface roughness, viscous dissipation and geometric imperfections of the microchannels, for example, can be considered separately in numerical model.

The aim of this numerical study is to analyze how the hydrodynamic and heat transfer characteristics can be affected by imperfections at the cross-section of the microchannels, in

single-phase laminar flow of a fluid with constant thermophysical properties. Other scaling effects, such as viscous dissipation and electrokinetic effect, for example, are not considered in the numerical model. The results obtained for single-phase laminar flow of water in microchannels with imperfections at the cross-section are compared to the ones obtained for a geometrically perfect microchannel through Poiseuille and Nusselt numbers. The results of this study were determined through mass conservation, Navier-Stokes and energy equations, by computational fluid dynamics (CFD).

2 COMPUTATIONAL MODEL

Computational models for the imperfect microchannels and the corresponding perfect microchannel of this study are based on the work by Steinke and Kandlikar [21] to a heatsink made up of an array of microchannels in a silicon substrate, which was used by Steinke et al. [48]. The perfect (ideal) microchannel of this study, called Microchannel 1, has a rectangular cross-section. Two imperfect microchannels were considered. One of these has rectangular cross-section whereas the other has a kind of a trapezoidal cross-section, these being the Microchannels 2 and 3, respectively. The outline cross-section geometry of these microchannels is shown in Figure 1.

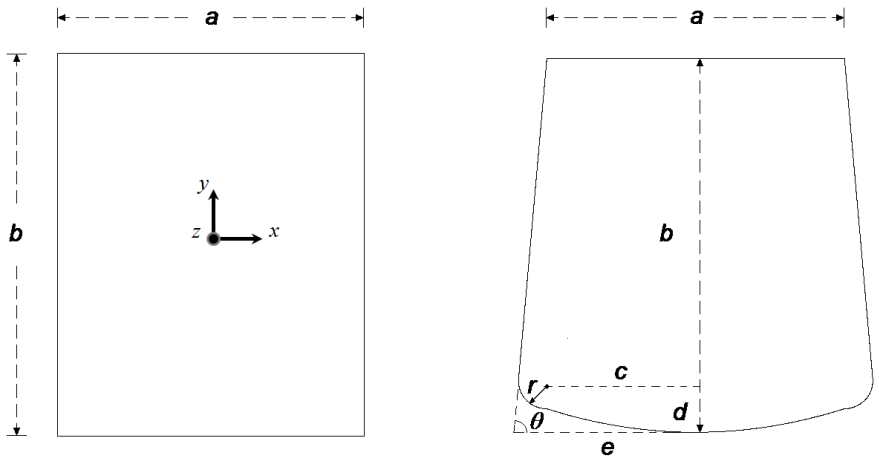

Figure 1: Scheme adopted for the computational model of the Microchannels (a) 1, 2 and (b) 3.

The Microchannel 1 consists of a tube with rectangular cross-section of width a = 200 µm and height b = 250 µm. The Microchannel 2 considers an inaccuracy in the measurements of the width and height of the cross-section of Microchannel 1, so that a = 201 µm and b = 247 µm. The Microchannel 3 consists of an tube with a kind of trapezoidal cross-section of a = 194 µm and b = 244 µm. At the bottom of the cross-section of it, the base is almost curved and with rounded corners. The channel walls form angle of θ = 85° with the horizontal. Other measurements indicated for Microchannel 3, in Figure 1(b), are c = 97 µm, d = 33.9 µm, e = 118.5 µm and r = 18.51 µm. The length L chosen for all microchannels was 0.223 m to ensure conditions of hydrodynamically and thermally developed flow near the outlet of the tubes ($L/D_h \cong 1{,}000$).

Table 1 shows the geometric details concerning the microchannels of this study.

Data	Microchannels		
	1	2	3
a [µm]	200	201	194
b [µm]	250	247	244
AR [-]	0.80	0.81	0.80
L [m]	0.223	0.223	0.223
Per [µm]	900.00	896.00	870.95
A_c [$\times 10^3$ µm^2]	50.00	49.65	50.76
A_s [$\times 10^6$ µm^2]	200.70	199.81	194.22
D_h [µm]	222.22	221.64	233.14
η [%]	0	− 0.26	+ 4.91

Table 1: Geometric parameters of the microchannels studied.

According to Table 1, the perimeter (Per) and surface area (A_s) of the Microchannel 3 are smaller than Microchannels 1 and 2. The cross-section area (A_c) of Microchannel 3 is higher than Microchannels 1 and 2. The same occurs for the relative deviation (η) on hydraulic diameter (D_h) of them. The aspect ratio (AR) of Microchannel 2 varied a little in relation to the Microchannels 1 and 3.

The values of a and b used for the Microchannel 2 were based on non-destructive measures of the cross-section of the heatsink studied by Steinke and Kandlikar [21]. According to the researchers, these measures refer to the values of the width and height of the cross-section of the microchannels obtained by optical measurement techniques. The values of a and b used for the Microchannel 3 are based on destructive measures of the heatsink, which was cleaved, according Steinke and Kandlikar [21]. After that, by the analysis of the images of its cross-section, obtained by a scanning electron microscope (SEM), the researchers found that the cross-section of the microchannels showed a kind of trapezoidal aspect, as shown in Figure 2.

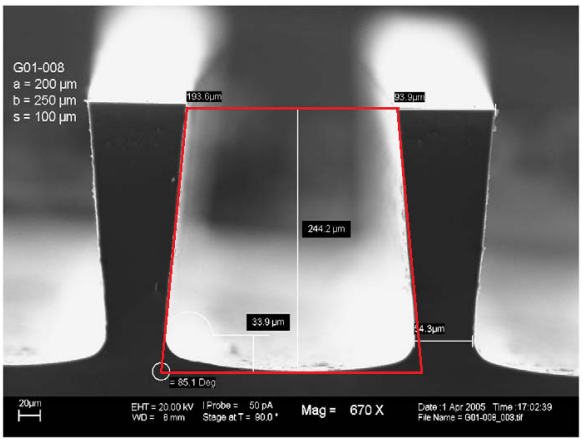

Figure 2: Image of the deformed cross-section of the microchannels of the heatsink studied by Steinke and Kandlikar [21].

In the original work by Steinke et al. [48], the microchannels were covered, on top of the cross-section, by a transparent cover of pyrex, which is not shown in Figure 2. An ideal trapezoid is indicated by red lines, for comparison with the deformed shape of the cross-section of the channel.

In all simulations, the working fluid chosen was water and the Reynolds numbers (Re) considered were 200, 400, 600 and 800, according to the work by Steinke and Kandlikar [21].

To transfer heat to fluid, it was considered a constant heat flux (q_s'') of 2 kW/m^2 applied on the surface of microchannels[1]. The entrance region of the microchannels was considered with simultaneous development of hydrodynamic and thermical boundary layers.

3 MATHEMATICAL MODEL

The fluid used is incompressible and with constant properties. The flow regime is laminar and permanent. Neither the viscous dissipation is considered, nor the gravitational effects. Based on these considerations, the equations of mass conservation, Eq. (1), Navier-Stokes, Eqs. (2-4), and energy, Eq. (5), in rectangular coordinates, are presented in the following:

$$\frac{\partial u}{\partial x}+\frac{\partial v}{\partial y}+\frac{\partial w}{\partial z}=0\,, \tag{1}$$

$$u\frac{\partial u}{\partial x}+v\frac{\partial u}{\partial y}+w\frac{\partial u}{\partial z}=-\frac{1}{\rho}\frac{\partial p}{\partial x}+\upsilon\left(\frac{\partial^2 u}{\partial x^2}+\frac{\partial^2 u}{\partial y^2}+\frac{\partial^2 u}{\partial z^2}\right), \tag{2}$$

$$u\frac{\partial v}{\partial x}+v\frac{\partial v}{\partial y}+w\frac{\partial v}{\partial z}=-\frac{1}{\rho}\frac{\partial p}{\partial y}+\upsilon\left(\frac{\partial^2 v}{\partial x^2}+\frac{\partial^2 v}{\partial y^2}+\frac{\partial^2 v}{\partial z^2}\right), \tag{3}$$

$$u\frac{\partial w}{\partial x}+v\frac{\partial w}{\partial y}+w\frac{\partial w}{\partial z}=-\frac{1}{\rho}\frac{\partial p}{\partial z}+\upsilon\left(\frac{\partial^2 w}{\partial x^2}+\frac{\partial^2 w}{\partial y^2}+\frac{\partial^2 w}{\partial z^2}\right), \tag{4}$$

$$u\frac{\partial T}{\partial x}+v\frac{\partial T}{\partial y}+w\frac{\partial T}{\partial z}=\alpha\left(\frac{\partial^2 T}{\partial x^2}+\frac{\partial^2 T}{\partial y^2}+\frac{\partial^2 T}{\partial z^2}\right), \tag{5}$$

where u, v and w are the velocity components of the fluid in the x, y and z directions, respectively, ρ, υ, α, p and T are the specific mass, the kinematic viscosity, the thermal diffusivity, the pressure and the temperature of the fluid, respectively.

The hydraulic diameter D_h is defined by

$$D_h=\frac{4A_c}{Per}\,. \tag{6}$$

For tubes with rectangular cross-section of width a and height b, the aspect ratio AR of its cross-section[2] is defined by

$$AR=\frac{a}{b}\,. \tag{7}$$

The Darcy friction factor f, the hydrodynamic resistance R_{hyd} and the hydrodynamic power P_{hyd} of the flow are defined, respectively, by

[1] In the study of Steinke and Kandlikar [21], the researchers studied only the hydrodynamic behavior of the flow, which was considered adiabatic. In the present study, looking forward to evaluate the impact of imperfections at the cross-section of the microchannels considered on the thermal behavior of the flow, it was decided to do an idealization. Therefore, it was considered a constant heat flux applied on the entire surface of the microchannels considered. Thus, it is possible to compare the results obtained to the local Nusselt number of this study with the theoretically predicted value [49] for this thermal condition.

[2] For tubes with trapezoidal cross-section, a in the Eq. (7) will be the smallest width of the cross-section [49].

$$f = \frac{2\rho D_h A_c^2 \Delta p}{\dot{m}^2 L}, \tag{8}$$

$$\Delta p = R_{hyd} Q, \tag{9}$$

and

$$P_{hyd} = \Delta p Q, \tag{10}$$

where Δp is the drop pressure and $\dot{m}$ is the mass flow rate, which is related to the volumetric flow rate Q by

$$\dot{m} = \rho Q = \rho w_m A_c, \tag{11}$$

where w_m is the mean velocity of flow.

The Poiseuille number Po and the Reynolds number Re are defined, respectively, as:

$$Po = f\,Re, \tag{12}$$

$$Re = \frac{\rho w_m D_h}{\mu}, \tag{13}$$

where μ is the dynamic viscosity of the fluid.

The shear stress τ on the walls of channels, in the region of hydrodynamically developed laminar flow, is related to the pressure gradient dp/dz and the hydraulic diameter D_h of channels by

$$\tau = \frac{1}{4} D_h \left(\frac{dp}{dz} \right). \tag{14}$$

The hydrodynamic entrance length L_{he} is defined by

$$L_{he} = 0.1\,Re\,D_h. \tag{15}$$

The local Nusselt number Nu is defined by

$$Nu = \frac{hD_h}{k}, \tag{16}$$

where k is the thermal conductivity of fluid and h is the local heat transfer coefficient, which is determined by

$$h = \frac{q_s''}{T_s - T_m} = \frac{1}{R_{ct}}, \tag{17}$$

where R_{ct} is the convection thermal resistance, T_s is the surface temperature of tubes and T_m is the mean temperature of fluid in cross-section, which is defined by

$$T_m = \frac{\int_{A_c} \rho w c_v T dA_c}{\dot{m} c_v}, \tag{18}$$

where c_v is the specific heat of fluid at constant volume.

The mean temperature gradient dT_m/dz for tubes with constant cross-section is defined by

$$\frac{dT_m}{dz} = \frac{q_s'' Per}{\dot{m} c_p}, \tag{19}$$

where c_p is the specific heat of fluid at constant pressure.

The total convection heat transfer rate q_{conv} for the tubes is defined by

$$q_{conv} = q_s'' A_s . \tag{20}$$

The thermal entrance length L_{te} is defined by

$$L_{te} = L_{he}\, Pr , \tag{21}$$

where Pr is the Prandtl number.

The magnitude of deviation ε of a generic variable Φ, in relation to the theoretical value expected for it, Φ_t, is determined by

$$\varepsilon_\Phi = \frac{|\Phi - \Phi_t|}{\Phi_t} \times 100\% , \tag{22}$$

whereas the deviation on the hydraulic diameter of the imperfect microchannels, related to the hydraulic diameter of the Microchannel 1, is particularly indicated by η (so that $\eta = \pm\varepsilon_{D_h}$).

The dimensionless height y^* of the cross-section of tubes is defined by

$$y^* = \frac{y}{b}, \tag{23}$$

whereas the dimensionless axial position z^* is given by

$$z^* = \frac{z}{L}. \tag{24}$$

The dimensionless local velocity in the flow direction w^* is defined by

$$w^* = \frac{w}{w_m} . \tag{25}$$

The dimensionless local temperature T^* is defined by

$$T^* = \frac{T - T_{m,i}}{\Delta T_m}, \tag{26}$$

where ΔT_m is the difference between the mean temperatures at outlet ($T_{m,o}$) and at inlet ($T_{m,i}$) of tubes.

4 NUMERICAL SOLUTION AND MESH INDEPENDENCE TEST

In the commercial software Ansys CFX-12, which was used to analyze the problem, the differential equations, Eqs. (1-5), were discretized and numerically solved for each point at the computational domain.

As a boundary condition to hydrodynamic problem, at the exits of all tubes a static pressure of 0 Pa was taken. At the entry of tubes a temperature of 293.15 K was taken and the velocity was computed according to the value of Reynolds number used in simulation. The temperature and the entry velocity were used as their initial field. The boundary condition on

the walls is with no slip and with a constant heat flux. The mesh used was hexahedral, with refinement next to the walls and also in the inlet and outlet sections of tubes. The error stability criterion used, for which the solution is taken as convergent, was 1×10^{-6}.

The determination of the number of elements for the meshes was made by analysis of *Po* and *Nu*. This analysis was performed for the case of flow with *Re* = 800, which provides the greatest thermal entrance length.

Table 2 shows the results of analysis for *Po* and *Nu*, and their respective numerical errors ε, for different meshes, for the Microchannel 1.

Mesh	Number of Elements	*Po* [-]	ε_{Po} [%]	*Nu* [-]	ε_{Nu} [%]
1	8,932	57.882491	0.612708	3.247690	5.069233
2	82,128	57.617176	0.151531	3.122779	1.028114
3	341,138	57.572184	0.073326	3.093280	0.073763
4	514,598	57.536471	0.011248	3.093279	0.073730
5	1,062,708	57.526555	0.005988	3.088316	0.086833
6	1,707,198	57.521075	0.015514	3.087702	0.106697
7	2,721,708	57.517642	0.021482	3.086934	0.131543

Table 2: Number of elements, *Po*, *Nu* and their respective numerical errors ε, for the Microchannel 1.

According with Table 2, the error analysis for Poiseuille number ε_{Po} shows that the result obtained by mesh 5 presented good agreement related to the theoretically provided value, $Po_t = 57.53$ [49], for tubes of rectangular cross-section with $AR = 0.8$. The error analysis for the local Nusselt number ε_{Nu} shows that the results obtained by meshes 3 and 4 presented the best accordance with the theoretical provided value, $Nu_t = 3.091$ [49], for tubes with rectangular cross-section with $AR = 0.8$. However, the analysis of ε_{Nu} for mesh 5 shows that the *Nu* of this mesh presented good agreement also with $Nu_t = 3.091$, when compared to the results obtained by other meshes. Thus, the refinement applied to mesh 5 was considered appropriate for this study (with *Po* = 57.53 and *Nu* = 3.09). The same was also applied to the Microchannel 2.

Table 3 shows the results of analysis for *Po* and *Nu*, and their respective numerical errors ε, for different meshes, for the Microchannel 3.

Mesh	Number of Elements	*Po* [-]	ε_{Po} [%]	*Nu* [-]	ε_{Nu} [%]
1	3,528	57.048818	0.836401	3.538608	14.481009
2	26,448	55.658113	3.253758	3.538455	14.476060
3	225,498	55.206327	4.039063	3.303791	6.884212
4	1,133,808	55.128093	4.175051	3.291820	6.496927
5	2,008,908	55.132183	4.167942	3.288696	6.395859
6	2,784,078	55.103206	4.218310	3.288623	6.393497
7	3,431,538	55.102080	4.220267	3.288478	6.388806

Table 3: Number of elements, *Po*, *Nu* and their respective numerical errors ε, for the Microchannel 3.

According with Table 3, the analysis of ε_{Po} shows that the results obtained by meshes from 4 to 7 didn't show very significant change related to the ones obtained by meshes from 1 to 3. The analysis of ε_{Nu} shows that the results obtained by meshes from 5 to 7 are almost independent of the refinement applied to them. Thus, the refinement applied to mesh 5 was considered appropriate for this study (with *Po* = 55.13 and *Nu* = 3.29).

As the analysis of ε_{Po} and ε_{Nu} for the Microchannel 3 was performed based on the theoretical values of Po_t e Nu_t concerning to the Microchannel 1, ε_{Po} is low for the mesh 1. It occurs because the Po of this mesh, which presents the lowest number of elements, is nearer Po_t concerning to the Microchannel 1. From mesh 2, Po is reduced as the refinement applied is increased until it reaches a value according to the imperfection at geometry of the cross-section of this tube.

Figure 3 shows an aspect of cross-section of the meshes selected to represent the microchannels of this study.

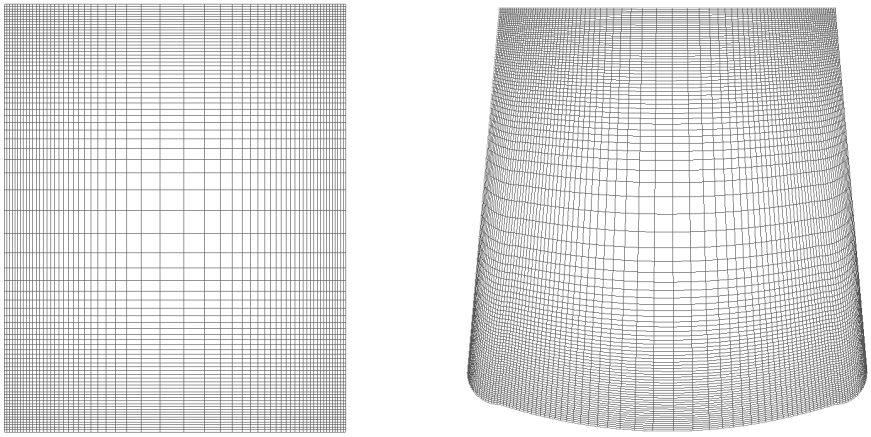

(a) (b)

Figure 3: Cross-section of the meshes selected to represent the Microchannels (a) 1, 2 and (b) 3.

Figure 3(a) shows the cross-section of meshes selected to represent the Microchannels 1 and 2, whereas the Figure 3(b) shows the cross-section of the mesh selected to represent the Microchannel 3. In both meshes, it can be noticed the high level of refinement applied on the wall of Microchannels to ensure the correct development of hydrodynamic and thermal boundary layers.

5 PROCEDURE ADOPTED

First, the thermophysical properties of water (ρ, μ, k, c_p and Pr) were based on the mean temperature of entrance of water ($T_{m,i}$) defined in numerical model, for the Reynolds number Re considered. Afterwards, the mean temperature of water in the outlet ($T_{m,o}$) of Microchannel 1 was determinated by mean temperature difference ΔT_m between the mean temperatures in the ends of this tube, which was obtained by integration of mean temperature gradient, Eq. (19), along the full length L of the tube. Thereby, all thermophysical properties of water were evaluated based on the mean temperature of reference $\overline{T}$ given by arithmetic average between the mean temperatures of water at inlet ($T_{m,i}$) and at outlet ($T_{m,o}$) of the tube. This procedure was performed iteratively until $\overline{T}$ didn't vary more significantly, assuming a convergence criterion of 0.1%. Then, the thermophysical properties of the fluid were considered constant and configured in the simulations, for both the Microchannel 1 and for the Microchannels 2 and 3.

The determination of Darcy friction factor f in region of hydrodynamically developed laminar flow, for the Microchannels, considered the drop pressure in this region, the length of this region ($L - L_{he}$) and the mass flow rate obtained from the simulations. The hydraulic diameter D_h and the cross-section area A_c used were the correspondents to the Microchannel 1.

Thus, according to Eq. (8), for the Microchannels 2 and 3 (imperfects), the deviations to Darcy friction factor f are due to changes in the drop pressure and mass flow rate, because of the imperfections in the cross-section area of the same ones. Therefore, the Poiseuille number Po is determined by Eq. (12) based on Darcy friction factor f obtained by Eq. (8).

The determination of local Nusselt number Nu in the region of thermally developed laminar flow ($L - L_{te}$), for all Microchannels, considered their local heat transfer coefficient h and the hydraulic diameter D_h of Microchannel 1. In the case of h, which is provided by Eq. (17), the surface temperature of microchannels T_s corresponds to average of the surface temperatures along the perimeter of the cross-section of the channels, at the axial position z considered. Therefore, the deviations for Nu at the imperfect microchannels are due to changes in h through the mean temperature T_m of the fluid in the cross-section and in the surface temperature T_s of these tubes, due to imperfections at the cross-section of these tubes.

6 RESULTS AND DISCUSSIONS

This section shows the results for Poiseuille Po and local Nusselt Nu numbers for the microchannels considered.

First, it is presented an analysis of the velocity and temperature profiles, in dimensionless form, for some dimensionless axial positions taken in the central plane of the channels (with $x = y = 0$), in the hydrodynamically and thermally developed flow, with $Re = 200$. The results related to the geometric, hydrodynamic and thermal quantities of flow in the tubes analysed are shown in table[3].

Subsequently, the results to Poiseuille Po and local Nusselt Nu numbers are shown, as well as deviations ε for the same ones, through graphics.

6.1 Velocity and Temperature Profiles

Figure 4 shows the velocity and temperature profiles for the Microchannels considered in the flow with $Re = 200$. For $z^* \cong 0.36$, 0.63, 0.90, Figure 4(a) shows the velocity profile, whereas Figures 4(b-d) show the temperature profile.

[3] The quantities determined in the region of hydrodynamically and thermally developed flow are indicated respectively by *hd* and *td* subscripts. However, some of these quantities were determined for the full length of tubes, including the hydrodynamic and thermal entrance effects. In this case, these quantities are indicated by their apparent value (subscript *app*), as occurs in some studies [21].

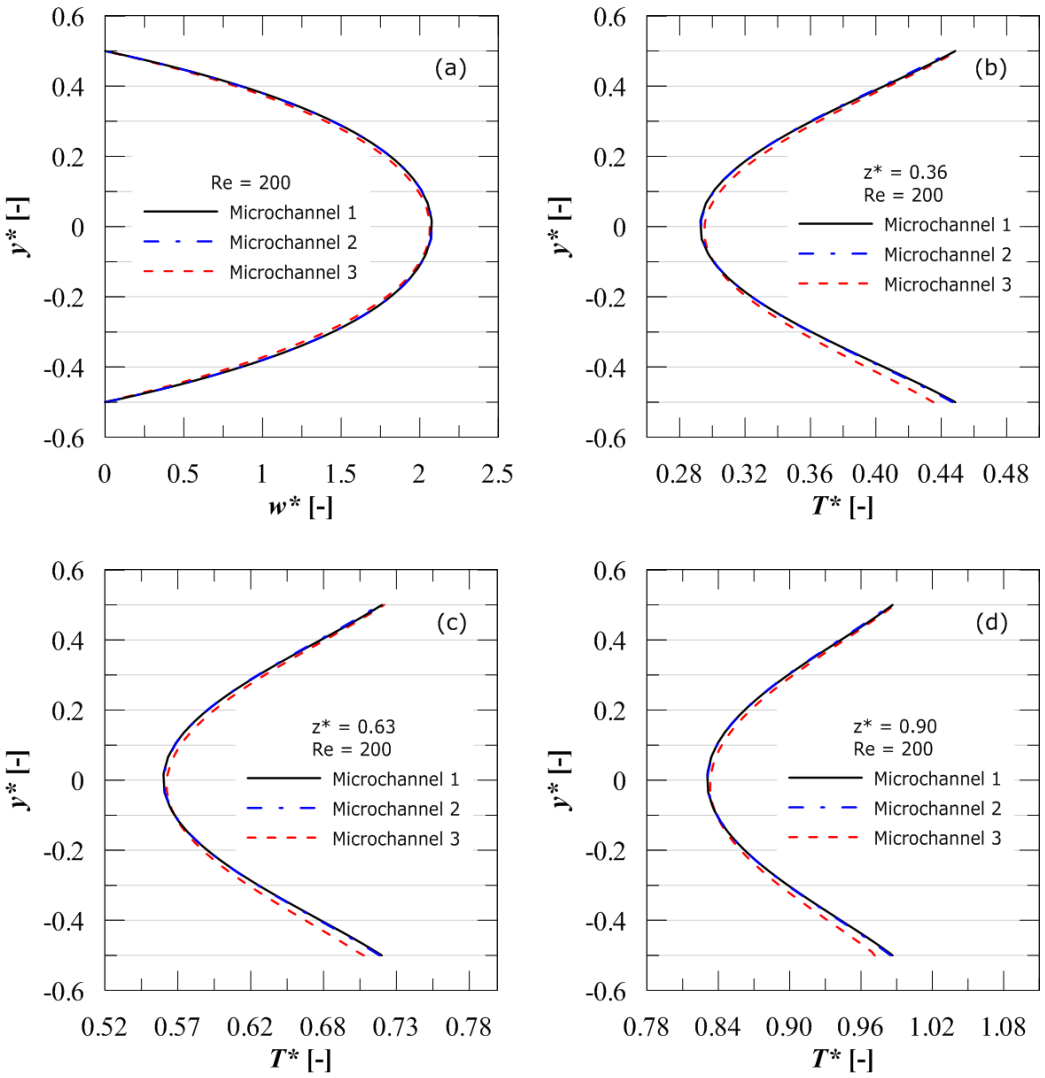

Figure 4: Microchannels with $Re = 200$ and $q_s'' = 2$ kW/m^2: Profiles of (a) velocity and (b-d) temperature in the central plane of the channels (with $x = y = 0$).

Figure 4(a) shows that the velocity profile for the Microchannel 2 is equal to the Microchannel 1, since its η was only –0.26%, according to Table 1. The velocity profile of Microchannel 3 is slightly closed, since its η was of +4.91%. It indicates that the mean velocity w_m in Microchannel 3 is lower than in Microchannels 1 and 2.

According to the temperature profiles in Figures 4(b-d), it is clear that they are perfectly symmetrical and basically identical for the Microchannels 1 and 2, and for similar reasons to those mentioned for the velocity profile in these tubes. However, it is observed that the temperature profiles of the Microchannel 3 are slightly distorted. They show that temperatures in the upper half of the cross-section of this tube are higher compared to ones in the lower half of its cross-section.

As shown in Figure 1(b) and in Figure 2, the irregularity of the perimeter of the cross-section of the Microchannel 3 shows a larger distribution of area in the lower half of the cross-section of this tube and reduced at the top of the channel. Thus, there is a greater amount of fluid flowing on the lower half of the cross-section of this tube. Hence, the fluid

heating should be lower in this region than in the upper half of the cross-section of this tube. Therefore, the fluid temperature in the lower half of the cross-section of this tube tends to be lower than in its upper half, as shown in temperature profiles of Figures 4(b-d).

Particularly, Figure 5 shows the velocity and temperature contours in the cross-section of the Microchannels 1 and 3[4] for $z^* \cong 0.36$, in the flow with $Re = 200$. Figures 5(a-b) show the velocity contours for the Microchannels 1 and 3, respectively, whereas Figures 5(c-d) show the temperature contours for the Microchannels 1 and 3, respectively.

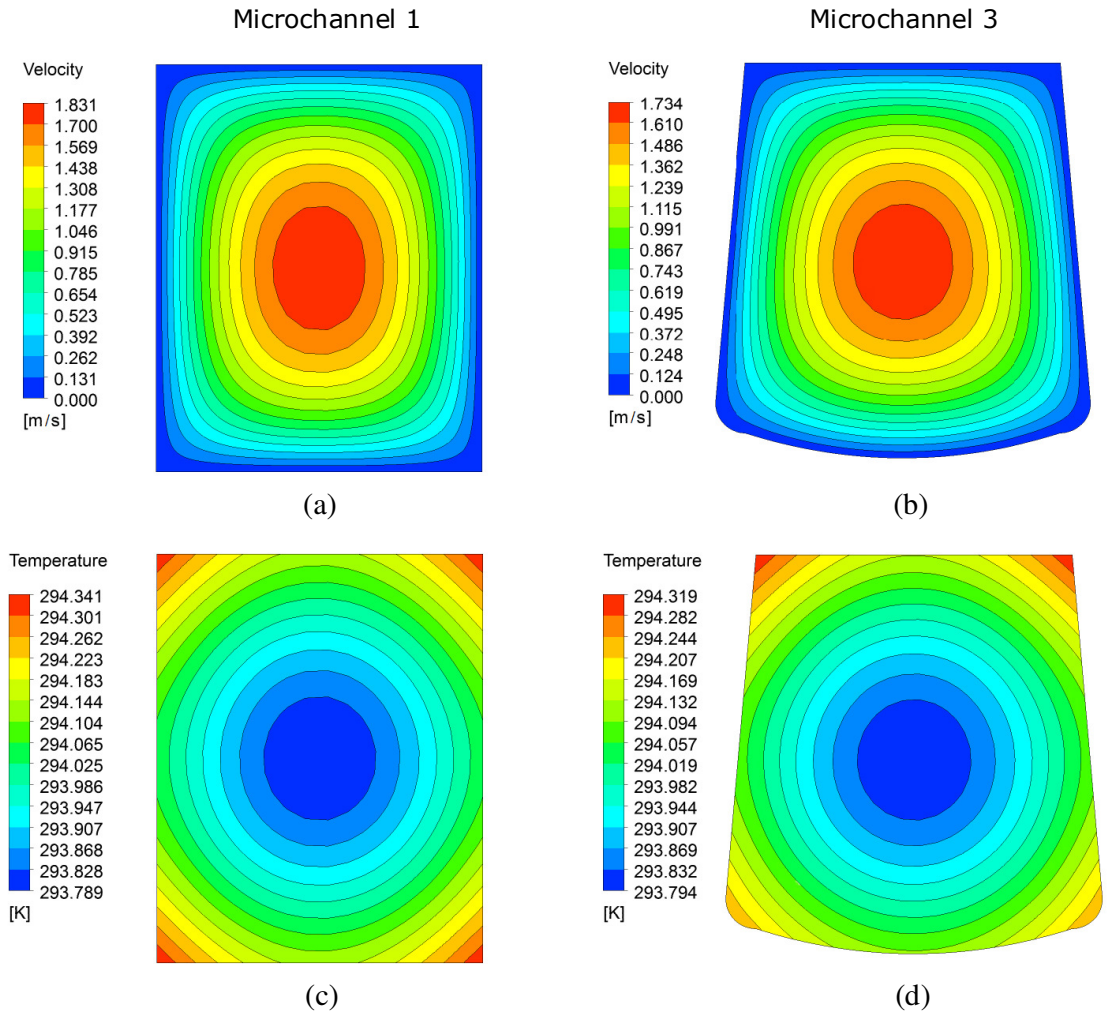

Figure 5: Contours of (a-b) velocity and (c-d) temperature in the cross-section of the Microchannels 1 and 3, respectively, in $z^* = 0.36$ with $Re = 200$.

As shown by velocity columns in Figures 5(a-b), the maximum velocity in Microchannel 3 is lower than in the Microchannel 1, as analyzed in the velocity profiles of Figure 4(a). Also, it can be seen clearly, as shown in Figure 5(d), that the temperatures at the upper half of the cross-section of the Microchannel 3 are higher compared to those in the lower half of its cross-section, as indicated in the analysis of temperature profiles of the Figures 4(b-d). As

[4] As the temperature and velocity profiles for Microchannel 1 and 2 are similar, as shown in Figure 4, it was decided to show only the velocity and temperature contours for the Microchannels 1 and 3 in order to make it easy to compare.

shown in Figure 5(d), the temperatures at the upper corners of the cross-section of the Microchannel 3 are higher compared to those in the lower corners of the cross-section of this channel. In the case of the Microchannel 1, the temperatures at its four corners of the cross-section are equal, as expected, according to Figure 5(c).

Table 4 shows the results concerning to the geometric, hydrodynamic and thermal quantities for the tubes considered in the flow with Re = 200.

Data	Microchannels		
	1	2	3
η [%]	0	–0.26	+4.91
w_m [m/s]	0.8802	0.8825	0.8391
D_h [μm]	222.22	221.64	233.14
Per [μm]	900.00	896.00	870.95
A_s [$\times 10^6$ μm^2]	200.70	199.81	194.22
A_c [$\times 10^3$ μm^2]	50.00	49.65	50.76
$(dp/dz)_{(hd)}$ [kPa/m]	500.37	503.56	448.95
$P_{hyd(app)}$ [mW]	4.93	4.94	4.28
$\Delta p_{(app)}$ [kPa]	112.05	112.76	100.52
Q [$\times 10^{-8}$ m^3/s]	4.40	4.38	4.26
$\dot{m}$ [$\times 10^{-5}$ kg/s]	4.39	4.37	4.25
$R_{hyd(app)}$ [$\times 10^{12}$ Pa s/m^3]	2.55	2.57	2.36
$\tau_{(hd)}$ [Pa]	27.78	27.88	26.15
$f_{(hd)}$ [-]	0.2876	0.2921	0.2755
dT_m/dz [K/m]	9.80	9.80	9.80
ΔT_m [K]	2.19	2.19	2.19
q_{conv} [mW]	401.40	399.62	388.51
$(T_s-T_m)_{(td)}$ [K]	0.25	0.24	0.23
$h(z)_{(td)}$ [kW/m^2 K]	8.16	8.19	8.70
$R_{ct}(z)_{(td)}$ [$\times 10^{-4}$ m^2 K/W]	1.23	1.22	1.15

Table 4: Microchannels with Re = 200 and q_s'' = 2 kW/m^2. Geometric, hydrodynamic and thermal quantities.

According to Table 4, the differences among the results obtained for the Microchannel 2 and the ones corresponding to the Microchannel 1 are minimal, as noted previously in Figure 4. As the cross-section area A_c of this tube is slightly smaller in relation to the one of Microchannel 1, there is a slight increase to the mean velocity of flow w_m, pressure gradient dp/dz, hydrodynamic power P_{hyd}, drop pressure Δp, hydrodynamic resistance R_{hyd}, shear stress τ and Darcy friction factor f, and a slight reduction to the mass flow rate $\dot{m}$ and volumetric flow rate Q in this tube. Then, the Poiseuille number Po in the Microchannel 2 should be slightly higher in relation to that one in Microchannel 1. As the convection thermal resistance R_{ct} in the Microchannel 2 is slightly lower than in the Microchannel 1, there is a small improvement in the heat transfer conditions to the fluid, as noted by analysis of the local heat transfer coefficient h, the difference between the surface and mean temperatures $(T_s–T_m)$ and the total convection heat transfer rate q_{conv} for the same one, relatively to Microchannel 1. So, the local Nusselt number Nu in Microchannel 2 should be a little higher in relation to the one in Microchannel 1.

Regarding to the Microchannel 3, the differences observed in the geometric, thermal and hydrodynamic results are more significant, compared to the ones corresponding to the Micro-

channel 1. As the A_c of the Microchannel 3 is somewhat larger in relation to the Microchannel 1, w_m, dp/dz, P_{hyd}, Δp, R_{hyd}, τ and f are somewhat smaller in the same one, compared to the ones of Microchannel 1. Therefore, the same must occur to Po. Furthermore, Table 4 shows that $\dot{m}$ and Q are lower in the Microchannel 3, although the A_c of the same one is larger than the one of Microchannel 1. In relation to heat transfer to the flow, the influence of the irregularity of the shape of the cross-section of the Microchannel 3, according to analysis of the temperature profiles in Figures 4(b-d), are quite noticeable too.

Table 4 indicates that h in the Microchannel 3 is higher in relation to the one of Microchannel 1. It is because the perimeter Per of the Microchannel 3 is smaller in comparison to the one of the Microchannels 1 and 2, as observed in Tables 1 and 4. Thereby, q_{conv} to the fluid is lower in Microchannel 3. Therefore, h is greater in Microchannel 3 in relation to that one in Microchannel 1. Consequently, the same should occur in relation to Nu.

The issue of heat transfer in Microchannel 3 is quite interesting. According to Table 5, the Microchannel 3, with $\eta > 0$, shows a higher h with lowest w_m, in relation to the Microchannels 1 and 2, although it shows the lowest q_{conv} of the channels considered. However, the A_c of the Microchannel 3 is larger compared to the one of Microchannel 1, which is not the case to Per and A_s of the same one. Then, the Microchannel 3 shows smaller q_{conv} even flowing a greater amount of fluid, compared to the other tubes. This is probably related to the irregular shape of the perimeter of the cross-section of this microchannel, which it is shown more influential in the process of heat transfer to the flow.

According to Table 4, it is noticed that dT_m/dz and ΔT_m are equal for all microchannels. By combining the Eqs. (6; 11; 13; 19), it is shown that the mean temperature gradient is defined by

$$\frac{dT_m}{dz} = \frac{\Delta T_m}{L} = \frac{4q_s''}{\mu Re c_p}, \tag{27}$$

which is constant for all microchannels, occurring the same to ΔT_m in these tubes.

6.2 Poiseuille Number

Figure 6 shows the results of Po according to Re for the tubes considered.

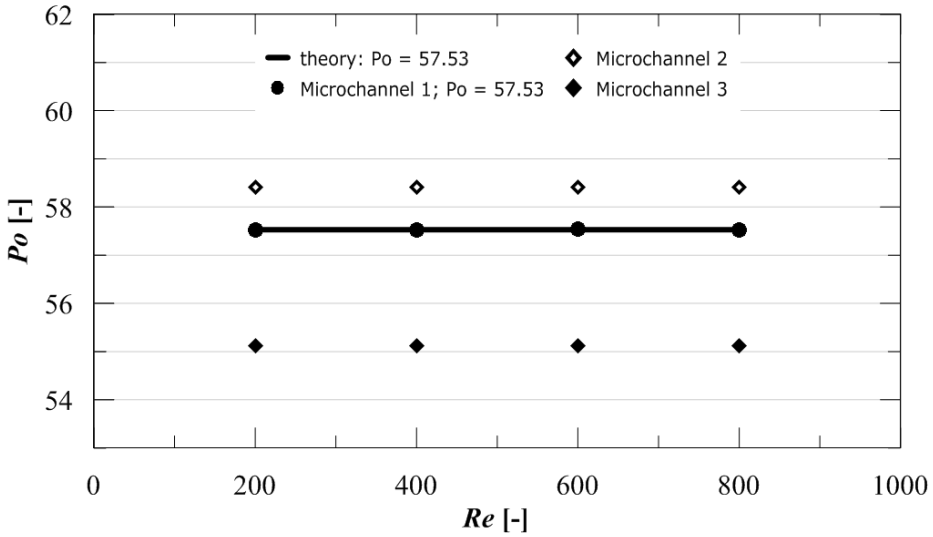

Figure 6: Poiseuille number vs. Reynolds number.

Figure 6 shows that Po in the Microchannel 2 exceeds slightly Po_t, whereas that it is considerably lower of Po_t in the Microchannel 3, as indicated previously, in the analysis of the Table 4.

Figure 7 shows the results of ε_{Po} according to Re for the tubes considered.

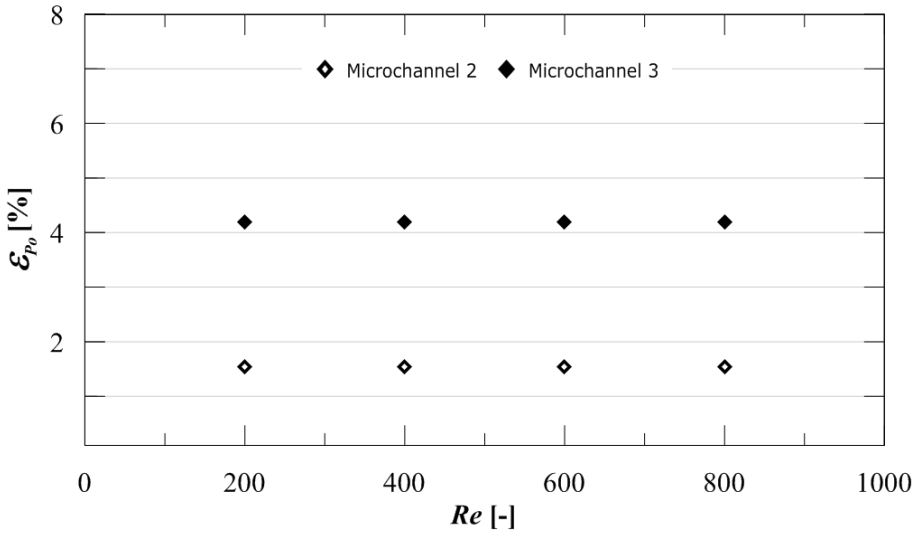

Figure 7: Deviation of Poiseuille number vs. Reynolds number.

Figure 7 shows that the results for ε_{Po} in the imperfect tubes were somewhat higher for the Microchannel 3, compared to the ones of the Microchannel 2, as expected.

The determination of f takes into account that the A_c of imperfect tubes is the same of the Microchannel 1. Considering the actual value of the A_c of the Microchannel 3 in Eq. (8), it is obtained ε_{Po} of about 1.25%. Taking into account also the real value of D_h of Microchannel 3 in Eq. (8), the ε_{Po} obtained for the same one increases to approximately 3.58%. However, if the Microchannel 3 is compared to a tube with perfect trapezoidal cross-section, such as that suggested by red lines in Figure 2, the results for Po can be in better agreement in this case, because for the hydrodynamically developed laminar flow in a tube with perfect trapezoidal cross-section, Po_t = 58 [49]. In this case, the result obtained for ε_{Po} in the Microchannel 3, considering its real A_c and D_h, comes to be approximately 2.75%, in relation to Po_t of the tube with perfect trapezoidal cross-section. As pointed out by Steinke and Kandlikar [21], this strengthens the fact that knowledge about the actual geometric shape of the cross-section of the tubes, as its width, height, Per and A_c, is very important for the correct determination of the hydrodynamic parameters of flow, as f and Po, at experimental level.

6.3 Nusselt Number

Figure 8 shows the results of Nu according to Re for the tubes considered.

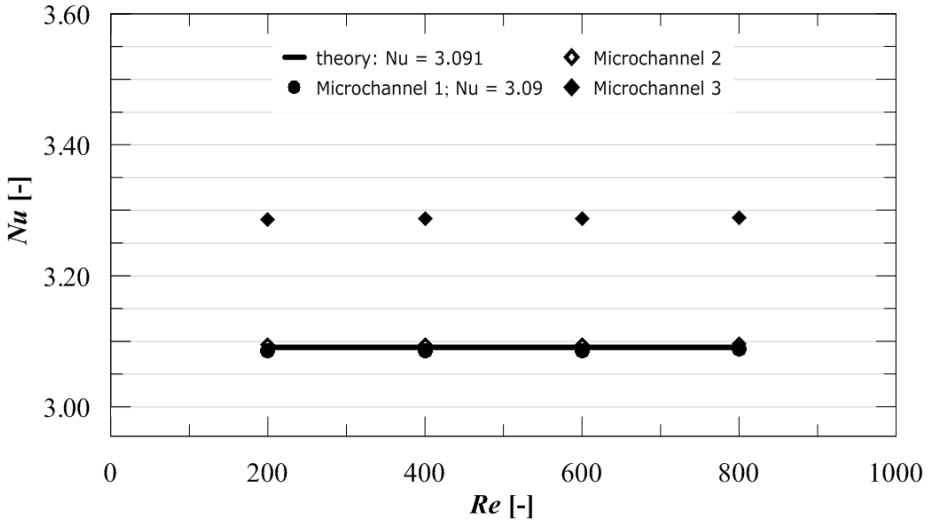

Figure 8: local Nusselt number vs. Reynolds number.

Figure 8 shows that Nu in the Microchannel 3 exceeds Nu_t, whereas that the same one is shown in perfect agreement to the Microchannel 2, as indicated previously, in the analysis of Table 4. The case of the Microchannel 3 indicates that Nu is more sensitive to the geometric shape of the cross-section of the microchannels, according to the reports of Croce and D'Agaro [45].

As the cross-section of the Microchannel 2 is the same nature (rectangular) as the cross-section of the Microchannel 1, and taking into account that their dimensions differed little from those of the Microchannel 1, Nu for the Microchannel 2 was in good agreement with the theoretical and numerical values corresponding to the Microchannel 1. However, the same didn't occur for Microchannel 3, since the cross-section of it is of trapezoidal nature. Thus, Nu = 3.29 for Microchannel 3 was in considerable disagreement with the theoretical and numerical values corresponding to the Microchannel 1, according to Figure 4. Even if the Microchannel 3 had been compared with a tube of perfect trapezoidal cross-section, as the ideal trapezoid indicated by red lines in Figure 2, the results for Nu may still not be in better agreement between themselves.

For thermally developed laminar flow in perfect trapezoid, indicated by red lines in Figure 2, assuming a length of 0.223 m for it and considering the thermal condition of constant heat flux applied on its surface, as in the tubes of this study, it is obtained that Nu_t = 3.05 [49], which is lower than the Nu_t = 3.091 of the Microchannel 1 with rectangular cross-section. Thus, Nu = 3.29 to the Microchannel 3 is still more discordant compared to Nu_t = 3.05 of the perfect trapezoid. However, this can be expected, since the perfect trapezoid has the highest Per and the highest A_s of the four tubes considered and, thus, the lowest Nu among these tubes. Therefore, the geometric shape of the cross-section is shown most influential in the process of heat transfer to the flow, as pointed out by Croce and D'Agaro [45].

Figure 9 shows the results of ε_{Nu} according to Re for the tubes considered.

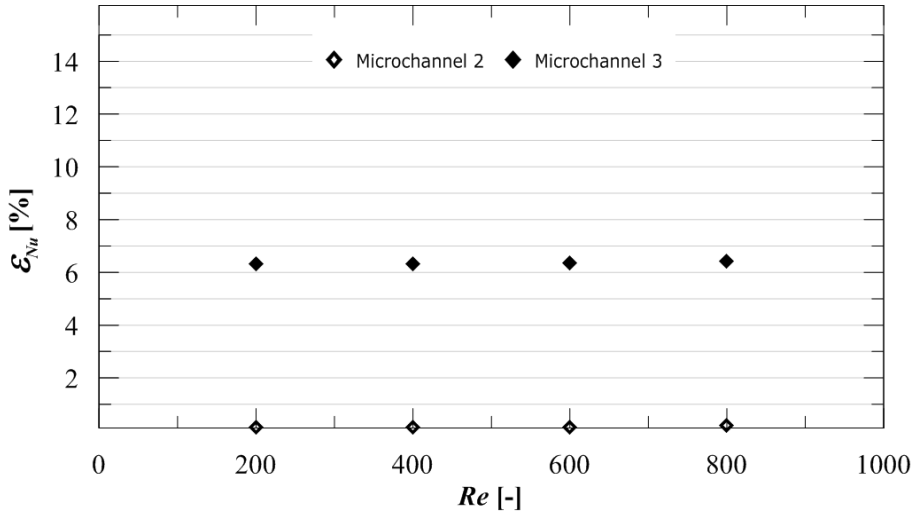

Figure 9: Deviation of local Nusselt number vs. Reynolds number.

As shown in Figure 9, the results for ε_{Nu} in Microchannel 2 are basically zero, whereas for the Microchannel 3 they are quite higher, as indicated in the analysis of Table 4.

7 CONCLUSIONS

The aim of this numerical study was to analyze how the hydrodynamic and heat transfer characteristics for the single-phase laminar flow in microscale, of a fluid with constant thermophysical properties, can be influenced by imperfections at the geometry of the microchannels, especially with respect to the cross-section of the same ones. For this purpose, all other scaling effects, such as surface roughness and viscous dissipation, for example, were omitted in the numerical model. It seeks to isolate and highlight the effects related only to the imperfections at the cross-section of microchannels on the hydrodynamic and thermal parameters of flow, as it is the case for Poiseuille and local Nusselt numbers, respectively. Although the simplifications considered in numerical model may overestimate the results founded, this study provided some general indications about the relative impacts to the imperfections at the cross-section on Poiseuille and Nusselt numbers in microchannels:

- The error at Poiseuille number can be reduced considering the real value of cross-section area of the microchannels, as pointed out in some experimental studies [21].
- The results of this study indicated that Nusselt number is more sensitive to shape of the cross-section of the microchannels, as pointed out in others numerical studies [45].

However, direct comparisons among experimental results and numerical results obtained in this study are not adequate. This is due to the experimental uncertainly present in the experimental data and the natural superposition of several different physical effects (of scaling), which were omitted in numerical model considered for this study, as well as other simplifications adopted for the same one.

Thus, more systematic numerical studies may be developed. Therefore, other models of imperfections at the cross-section of the microchannels should be considered.

8 ACKNOWLEDGMENTS

The authors acknowledge the Conselho Nacional de Desenvolvimento Científico e Tecnológico (CNPq) and Universidade do Vale do Rio dos Sinos (UNISINOS) for financial support for this work.

REFERENCES

[1] G.P. Celata, M. Cumo, G. Zummo, Thermal-hydraulic characteristics of single-phase flow in capillary pipes. *Experimental Thermal and Fluid Science*, **28**, 87–95, 2004.

[2] G.P. Celata, M. Cumo, V. Marconi, S.J. McPhail, G. Zummo, Microtube liquid single-phase heat transfer in laminar flow. *International Journal of Heat and Mass Transfer*, **49**, 3538–3546, 2006.

[3] P. Tabeling, Introduction to Microfluidics. *New York: Oxford University Press*, 2005.

[4] P. Rosa, T.G. Karayiannis, M.W. Collins, Single-phase heat transfer in microchannels: The importance of scaling effects. *Applied Thermal Engineering*, **29**, 3447–3468, 2009.

[5] H.C. Chiu, J.H. Jang, H.W. Yeh, M.S, Wu, The heat transfer characteristics of liquid cooling heatsink containing microchannels. *International Journal of Heat and Mass Transfer*, **54**, 34–42, 2011.

[6] P.Y. Wu, W.A. Little, Measurement of heat transfer characteristics of gas flow in fine channel heat exchangers used for microminiature refrigerators. *Cryogenics*, **24**, 415–420, 1984.

[7] J. Pfahler, J. Harley, H. Bau, J. Zemel, Liquid Transport in Micron and Submicron Channels. *Sensors and Actuators A: Physical*, **22**, 431–434, 1990.

[8] J. Pfahler, J. Harley, H. Bau, J. Zemel, Gas and Liquid Flow in Small Channels. *Micromechanical Sensors, Actuators, and Systems, ASME*, **32**, 49–60, 1991.

[9] S.B. Choi, R.F. Barron, R.O. Warrington, Fluid Flow and Heat Transfer in Microtubes. *Micromechanical Sensors, Actuators, and Systems, ASME*, **32**, 123–134, 1991.

[10] D. Yu, R. Warrington, R. Barron, T. Ameel, An experimental and theoretical investigation of fluid flow and heat transfer in microtubes. *In: Proceedings of ASME/JSME Thermal Engineering Conference*, **1**, 523–530, 1995.

[11] D. Pfund, D. Rector, A. Shekarriz, A. Popescu, J.R. Welty, Pressure Drop Measurements in a Microchannel. *AIChE Journal*, **46**, 1496–1507, 2000.

[12] G.M. Mala, D. Li, Flow characteristics of water in microtubes. *International Journal of Heat and Fluid Flow*, **20**, 142–148, 1999.

[13] B. Xu, K.T. Ooi, N.T. Wong, W.K. Choi, Experimental investigation of flow friction for liquid flow in microchannels. *International Communications in Heat and Mass Transfer*, **27**, 1165–1176, 2000.

[14] Z.X. Li, D.X. Du, Z.Y. Guo, Experimental study on flow characteristics of liquid in circular microtubes. *In: Proceedings of the International Conference on Heat Transfer and Transport Phenomena in Microscale*, Banff, Canada, October 15-20, 2000.

[15] G. Tunc, Y. Bayazitoglu, Heat transfer in microtubes with viscous dissipation. *International Journal of Heat and Mass Transfer*, **44**, 2395–2403, 2001.

[16] J. Judy, D. Maynes, B.W. Webb, Characterization of frictional pressure drop for liquid flows through Microchannels. *International Journal of Heat and Mass Transfer*, **45**, 3477–3489, 2002.

[17] H.Y. Wu, P. Cheng, An Experimental Study of Convective Heat Transfer in Silicon Microchannels with Different Surface Conditions. *International Journal of Heat and Mass Transfer*, **46**, 2547–2556, 2003.

[18] G.P. Celata, M. Cumo, M. Guglielmi, G. Zummo, Experimental Investigation of Hydraulic and Single-Phase Heat Transfer in 0.130 mm Capillary Tube. *Microscale Thermophysical Engineering*, **6**, 85–97, 2002.

[19] G.P. Celata, M. Cumo, S.J. McPhail, G. Zummo, Characterization of fluid dynamic behaviour and channel wall effects in microtube. *International Journal of Heat and Fluid Flow*, **27**, 135–143, 2006.

[20] G.P. Celata, G.L. Morini, V. Marconi, S.J. McPhail, G. Zummo, Using viscous heating to determine the friction factor in microchannels – An experimental validation. *Experimental Thermal and Fluid Science*, **30**, 725–731, 2006.

[21] M.E. Steinke, S.G. Kandlikar, Single-phase liquid friction factors in microchannels. *International Journal of Thermal Sciences*, **45**, 1073–1083, 2006.

[22] G.M. Mala, D. Li, J.D. Dale, Heat transfer and fluid flow in microchannels. *International Journal of Heat and Mass Transfer*, **40**, 3079–3088, 1997.

[23] C. Yang, D. Li, J.H. Masliyah, Modeling forced liquid convection in rectangular microchannels with electrokinetic effects. *International Journal of Heat and Mass Transfer*, **41**, 4229–4249, 1998.

[24] C.P. Tso, S.P. Mahulikar, The use of the Brinkman number for single phase forced convective heat transfer in microchannels. *International Journal of Heat and Mass Transfer*, **41**, 1759–1769, 1998.

[25] K.C. Toh, X.Y. Chen, J.C. Chai, Numerical computation of fluid flow and heat transfer in microchannels. *International Journal of Heat and Mass Transfer*, **45**, 5133–5141, 2002.

[26] J. Koo, C. Kleinstreuer, Viscous dissipation effects in microtubes and Microchannels. *International Journal of Heat and Mass Transfer*, **47**, 3159–3169, 2004.

[27] J. Koo, C. Kleinstreuer, Analysis of surface roughness effects on heat transfer in microconduits. *International Journal of Heat and Mass Transfer*, **48**, 2625–2634, 2005.

[28] G. Gamrat, M. Favre-Marinet, D. Asendrych, Conduction and entrance effects on laminar liquid flow and heat transfer in rectangular Microchannels. *International Journal of Heat and Mass Transfer*, **48**, 2943–2954, 2005.

[29] P.S. Lee, S.V. Garimella, D. Liu, Investigation of heat transfer in rectangular microchannels. *International Journal of Heat and Mass Transfer*, **48**, 1688–1704, 2005.

[30] T.Y. Lin, C.Y. Yang, Measurement of micro-tube surface temperature by the method of liquid crystal thermograph. *In: 6th World Conference on Experimental Heat Transfer, Fluid Mechanics, and Thermodynamics*, Matsushima, Japan, April 17-21, 2005.

[31] C.Y. Yang, T.Y. Lin, Heat transfer characteristics of water flow in microtubes. *Experimental Thermal and Fluid Science*, **32**, 432–439, 2007.

[32] T.Y. Lin, C.Y. Yang, S.G. Kandlikar, Measurement of heat transfer in the entrance region of small diameter tubes. *In: Proceedings of the ASME 2009, 7th International Conference on Nanochannels, Microchannels and Minichannels*, Pohang, South Korea, June 22-24, 2009.

[33] C.Y. Yang, C.W. Chen, T.Y. Lin, S.G. Kandlikar, Heat transfer and friction characteristics of air flow in microtubes. *Experimental Thermal and Fluid Science*, **37**, 12–18, 2012.

[34] X.F. Peng, B.X. Wang, Forced convection and flow boiling heat transfer for liquid flowing through microchannels. *International Journal of Heat and Mass Transfer*, **36**, 3421–3427, 1993.

[35] B.X. Wang, X.F. Peng, Experimental investigation on liquid forced-convection heat transfer through microchannels. *International Journal of Heat and Mass Transfer*, **37**, 73–82, 1994.

[36] X.F. Peng, B.X. Wang, G.P. Peterson, H.B. Ma, Experimental investigation of heat transfer in flat plates with rectangular microchannels. *International Journal of Heat and Mass Transfer*, **38**, 127–137, 1995.

[37] G. Maranzana, I. Perry, D. Maillet, Mini- and micro-channels: influence of axial conduction in the walls. *International Journal of Heat and Mass Transfer*, **47**, 3993–4004, 2004.

[38] I. Tiselj, G. Hetsroni, B. Mavko, A. Mosyak, E. Pogrebnyak, Z. Segal, Effects of axial conduction on the heat transfer in micro-channels. *International Journal of Heat and Mass Transfer*, **47**, 2551–2565, 2004.

[39] G.P. Celata, M. Cumo, S.J. McPhail, G. Zummo, Single-phase laminar and turbulent heat transfer in smooth and rough microtubes. *Microfluid Nanofluid*, **3**, 697–707, 2007.

[40] D. Lelea, A.E. Cioabla, The viscous dissipation effect on heat transfer and fluid flow in micro-tubes. *International Communications in Heat and Mass Transfer*, **37**, 1208–1214, 2010.

[41] G.L. Morini, Viscous heating in liquid flows in micro-channels. *International Journal of Heat and Mass Transfer*, **48**, 3637–3647, 2005.

[42] P.L. Young, S.G. Kandlikar, Surface roughness effects on heat transfer in microscale single phase. *In: Proceedings of the Sixth International ASME Conference on Nanochannels, Microchannels and Minichannels*, Darmstadt, Germany, June 23-25, 2008.

[43] C.H. Chen, Forced convection heat transfer in microchannel heat sinks. *International Journal of Heat and Mass Transfer*, **50**, 2182–2189, 2007.

[44] G. Hetsroni, A. Mosyak, E. Pogrebnyak, L.P Yarin, Heat transfer in microchannels: Comparison of experiments with theory and numerical results. *International Journal of Heat and Mass Transfer*, **48**, 5580–5601, 2005.

[45] G. Croce, P. D'agaro, Numerical analysis of roughness effect on microtube heat transfer. *Superlattices and Microstructures*, **35**, 601–616, 2004.

[46] G. Croce, P. D'agaro, C. Nonino, Three-dimensional roughness effect on microchannel heat transfer and pressure drop. *International Journal of Heat and Mass Transfer*, **50**, 5249–5259, 2007.

[47] P.S. Lee, S.V. Garimella, Thermally developing flow and heat transfer in rectangular microchannels of different aspect ratios. *International Journal of Heat and Mass Transfer*, **49**, 3060–3067, 2006.

[48] M.E. Steinke, S.G. Kandlikar, J.H. Magerlein, E.G. Colgan, A.D. Raisanen, Development of an Experimental Facility for Investigating Single-Phase Liquid Flow in Microchannels. *Heat Transfer Engineering*, **27**, 41–52, 2006.

[49] R.K. Shah, A.L. London, Laminar flow forced convection in ducts: a source book for compact heat exchanger analytical data. *New York: Academic Press*, 1978.